Supplementary Information

Janus-interface engineering boosting solar steam towards high-efficiency water collection

Houze Yao,[a] Panpan Zhang,[a] Ce Yang,[a] Qihua Liao,[ad] Xuanzhang Hao,[a] Yaxin Huang,[a] Miao Zhang,[b] Xianbao Wang,[c] Tengyu Lin, [ad] Huhu Cheng, *[a] Jiayin Yuan *[b] and Liangti Qu *[a]

a. State Key Laboratory of Tribology, Department of Mechanical Engineering, and Key Laboratory of Organic Optoelectronics & Molecular Engineering, Ministry of Education, Department of Chemistry, Tsinghua University, Beijing 100084, P. R. China.

b. Department of Materials and Environmental Chemistry, Stockholm University, 10691, Stockholm, Sweden

c. Key Laboratory for the Green Preparation and Application of Functional Materials, Ministry of Education, Hubei Key Laboratory of Polymer Materials, School of Materials Science and Engineering, Hubei University, Wuhan 430062, P. R. China

d. HurRain Nano Technology Co., Ltd, Beijing 100084, P. R. China.

Corresponding author:

lqu@mail.tsinghua.edu.cn (L. Qu), huhucheng@tsinghua.edu.cn (H. Cheng),

jiayin.yuan@mmk.su.se (J. Yuan)

Supplementary Methods

Preparation of ACPA. All reagents and raw materials were commercially available. The concentration of the chitosan solution (Macklin) is 20 mg mL^{-1}. Typically, 2 mL of glacial acetic acid was added into 96 mL of de-ionized water, and then 2 g of chitosan was dispersed in the suspension under vigorous stirring. The precursor solution of ACPA was prepared by adding a different volume of PVA (Macklin, 1788) solution (100 mg mL^{-1}) into 10 mL of chitosan solution (20 mg mL^{-1}). In a typical example, 0.2 mL PVA solution was added to get a PVA/chitosan mixture (10%, w/w) solution. Then water was added to make the final concentration of chitosan at 10 mg mL^{-1}. The weight ratio (PVA/chitosan) can be controlled in the range from 0 to 0.30. The PVA/chitosan solutions with different weight ratios were mixed with ethanol under sonication (30:1, v/v), and transferred into a plastic mold. After being frozen by liquid nitrogen, the PVA/chitosan matrix was freeze-dried for 48 h and then treated in an oven at 80 ºC for 4 hours to prepare the chitosan/PVA aerogel. After completely dried, the aerogel was treated with a mixed solution ($V_{methanol}$: $V_{acetic\ anhydride}$ = 10: 1) at 50 ºC for 4 h. After repeated washing with ethanol and deionized water, and finally drying in air, the ACPA was obtained.

Preparation of the evaporation side of J-SSG. A copper foam was welded to copper foil. The copper foam side was immersed in the above-mentioned PVA/chitosan solution and sonicated for 30 min. Then the copper foam was taken out and the solution was applied to the inside of the foam. The remaining steps are the same as the preparation of ACPA.

Fabrication of the solar absorption side of J-SSG. A HGTECH LSU3EA laser system (355 nm, 30 kHz) was utilized for the micro−nano fabrication procedure. Before laser processing, the copper (99.9% purity) was mechanically polished to mirror finish and cleaned by sonication with ethanol to remove the oxide and grease on their surfaces. The laser power is 3 W, and the scanning speed is 10 mm s^{-1}. In the case of under focus, x-y arrays with 50 micrometer line spacing were printed in air. Subsequently, the sonication treatment in ethanol was used to remove the attached particles.

Solar water evaporation and solar water production experiment. In both tests, the water is supplied through a commercial pump. Before the test, J-SSG is pre-soaked in water, and no water flows out by gravity when it is placed vertically. In the evaporation test, by calculating the water supply volume and the overflow volume of the water in the J-SSG, the water evaporation volume is obtained. In the water production test, we use the optimized water supply. After the one-hour test, the water collected by the desalination system was weighed. The thermocouple is in contact with the evaporator and condenser by welding to measure the surface temperature in real-time. The water evaporation and production rate test results are the average of three tests.

Preparation of superhydrophobic aluminum condenser. First, the polished aluminum foil was immersed into the hydrochloric acid and copper sulfate mixture solution (0.1 mol/L HCl and 0.1 mol/L $CuSO_4$) for 5 min. After immersion in deionized water and drying, the aluminum foil was immersed into a fluoroalkylsilane (1H,1H,2H,2H-perfluorodecyltriethoxysilane, Meryer, >96%) solution (1 wt%) for 30 min. Finally, the aluminum foil was taken out and dried in a drying oven at 100 ºC for an hour, and the superhydrophobic aluminum condenser was obtained.

Materials Characterizations. The morphological structures were characterized by scanning electron microscopy (Gemini 300). Fourier-transform infrared spectroscopy (FT-IR) spectra were collected on a UATR Two FT-IR spectrometer. Thermogravimetric analysis was performed by using a thermogravimetric analyzer (TGA/DSC, STA449F3) under air, and the heating rate was 10 K min^{-1}. The temperature distribution was recorded using an IR camera (Fluke TiX640) in real-time. The temperature is measured by welding a thermocouple on the surface. The ion concentrations of water were performed by the inductively coupled plasma (ICP) emission spectrometer (Vista-MPX). The thermal diffusivity of the material is measured by the laser flash method (LFA467). The optical transmittance and reflectance spectra of the aerogel were measured on a varian UV-Vis spectrophotometer (Cary 7000) with an Agilent integrating sphere. The solar intensity is measured by a reference cell and meter (91150V, Newport). All weights were measured by analytical balance (METTLER TOLEDO ME104E).

Supplementary Figures

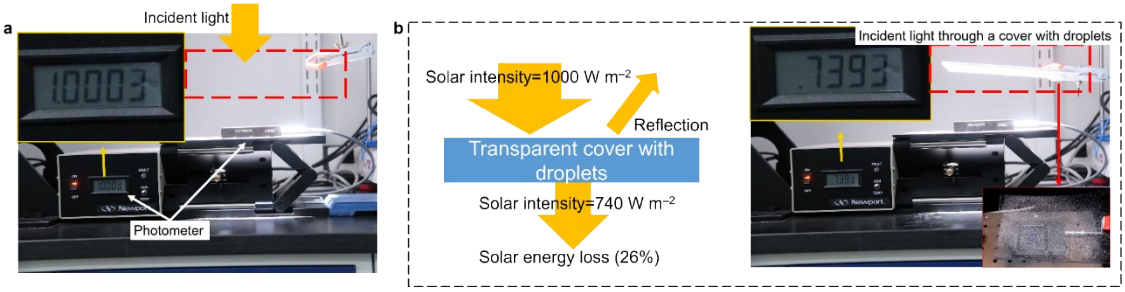

Figure S1. (a) The incident light directly shines on the photometer, and the solar intensity is 1000 W m^{-2}. (b) The incident light shines on the photometer through a transparent cover (commercial polymethylmethacrylate, PMMA) with droplets, and the solar intensity is 739 W m^{-2}. Thus, the total solar energy loss is about 26%. The inset shows the PMMA sheet with droplets covering the photometer.

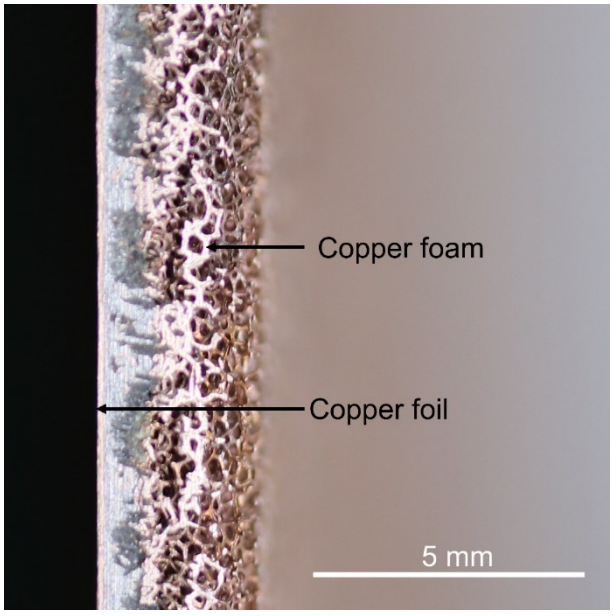

Figure S2. Cross-sectional photograph of the home-made Janus-type copper foil/foam skeleton. The copper foam is directly welded to copper foil.

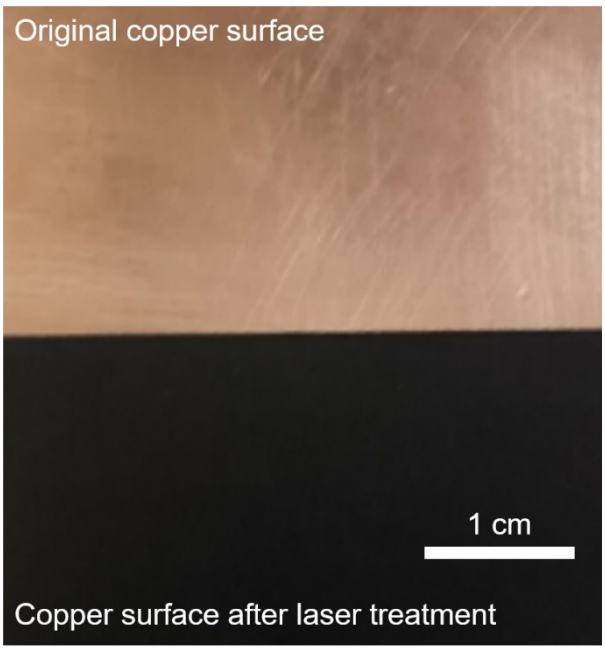

Figure S3. The photograph shows the copper foil surface before and after laser treatment.

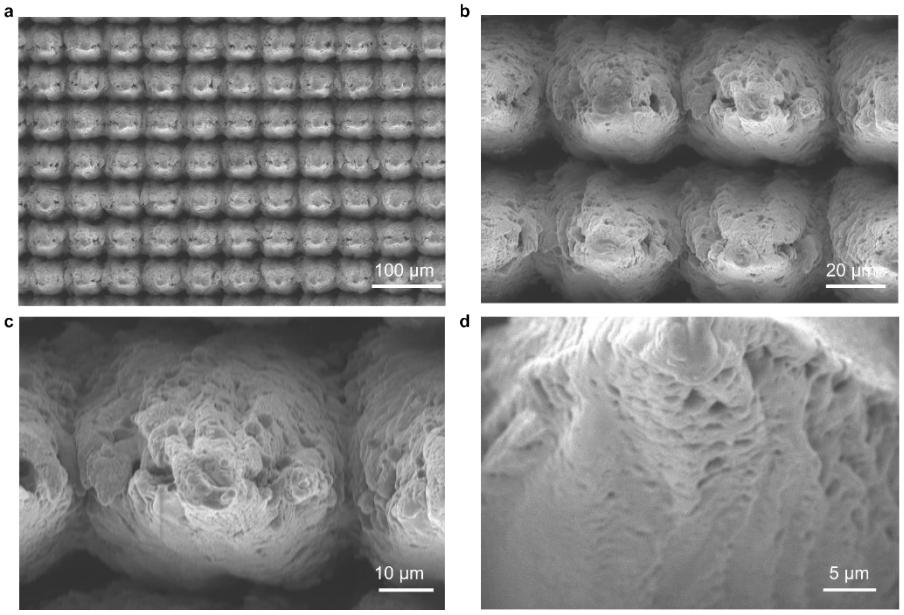

Figure S4. SEM photographs of the micro-nano hybrid antireflection structures on copper foil for the light-absorbing surface at different magnifications.

Note S1 Calculation of solar-thermal conversion efficiency.

For a material under thermal equilibrium, the heat absorption power $P_{absorption}$ is equal to the heat dissipation power $P_{dissipation}$[1]. Therefore, the solar-thermal conversion efficiency α of the solar absorption side of J-SSG can be calculated by the following formula:

$$\alpha = \frac{P_{absorption}}{P_{solar}} = \frac{P_{dissipation}}{P_{solar}}$$

By measuring the real-time temperature change of the J-SSG under natural heat dissipation (Supplementary Fig. 5), its heat dissipation power at any temperature can be obtained by the following formula:

$$P_{dissipation} = \frac{dT_{scl}}{dt} C_{v-scl}$$

Where, T_{scl} is the temperature of the solar absorption side and C_{v-scl} is the heat capacity of J-SSG.

The solar-thermal conversion efficiency under different incident angles is calculated as shown in Supplementary Figure 6.

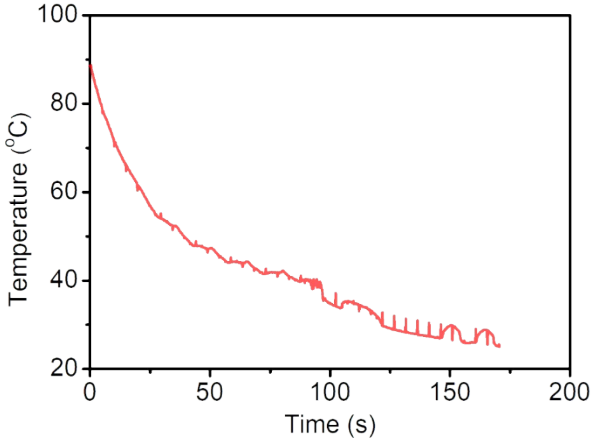

Figure S5. The temperature change of J-SSG under natural heat dissipation.

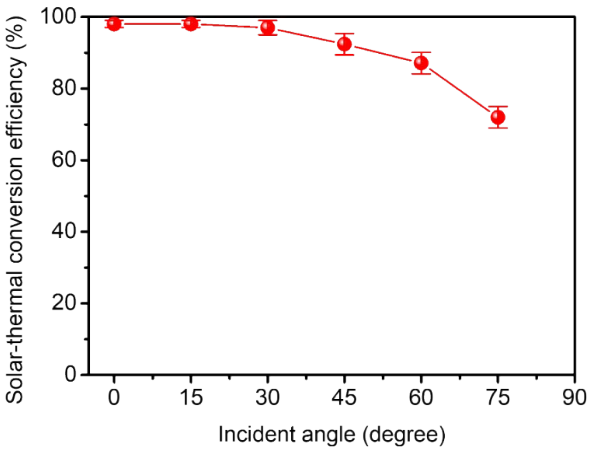

Figure S6. The solar-thermal conversion efficiency of the absorber of J-SSG under different incident angles.

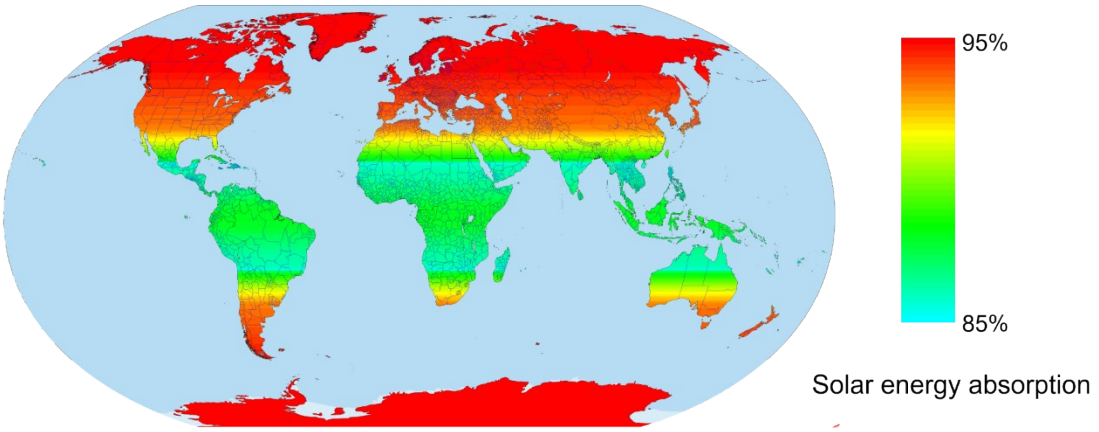

Figure S7. The annual average solar energy absorption of J-SSG on earth, based on the global annual solar zenith angle distribution[2] and the light absorption performance of J-SSG at different incident angles. The solar energy absorption is calculated by integrating the incident angle distribution at different latitudes and the corresponding J-SSG absorption.

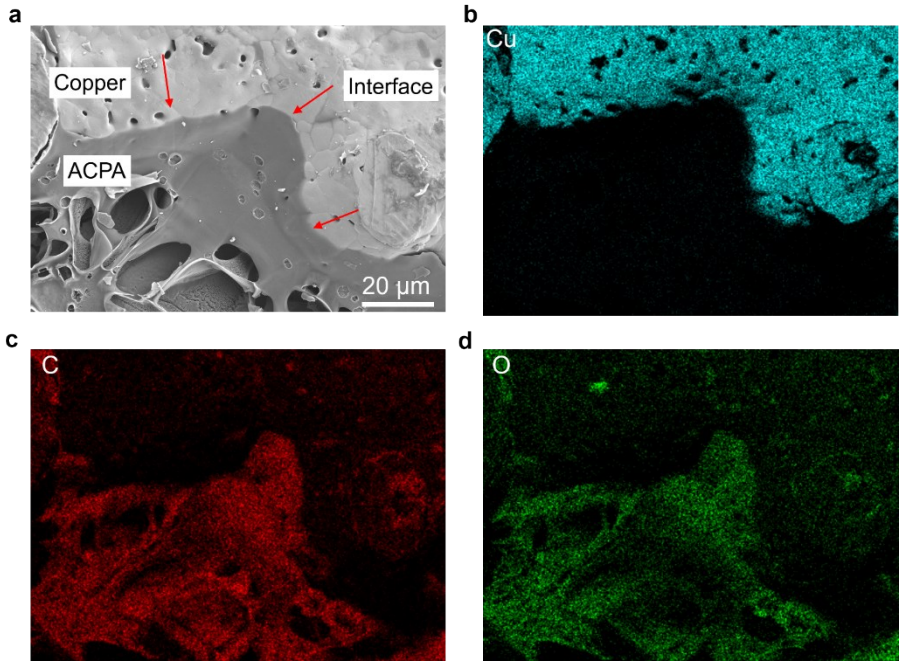

Figure S8. SEM photograph (a) and energy-dispersive X-ray spectroscopy (b–d) of the copper/ACPA interface. Corresponding distribution maps of (b) Cu, (c) C, and (d) O elements, which demonstrates the good combination between ACPA and copper at the boundary. During the preparation of water evaporation side of J-SSG, the PVA/chitosan precursor solution is first filled in the porous copper foam under the capillary force before freeze-drying process, which cannot be over the edge of the copper foam.

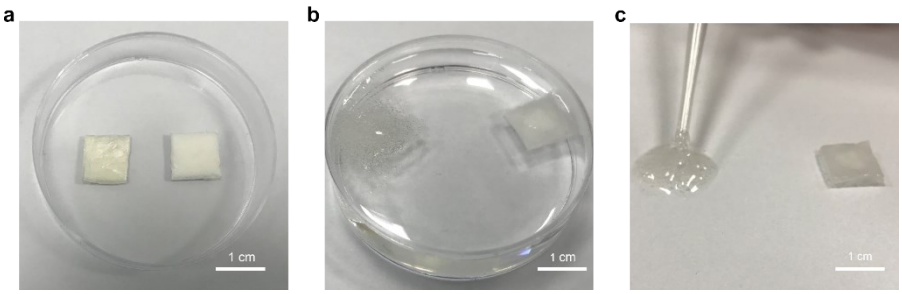

Figure S9. (a) Chitosan/PVA aerogel (left) and ACPA (right). (b) and (c) Chitosan/PVA aerogel swells and is destroyed in water. ACPA keeps the structure stable in water after 6 months.

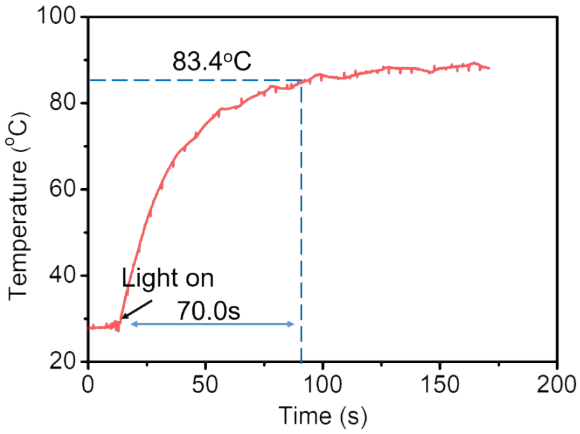

Figure S10. The temperature change of J-SSG under one sun irradiation. The whole J-SSG can reach ~83.4 ºC after irradiating the solar absorber side under one sun irradiation for 70.0 s.

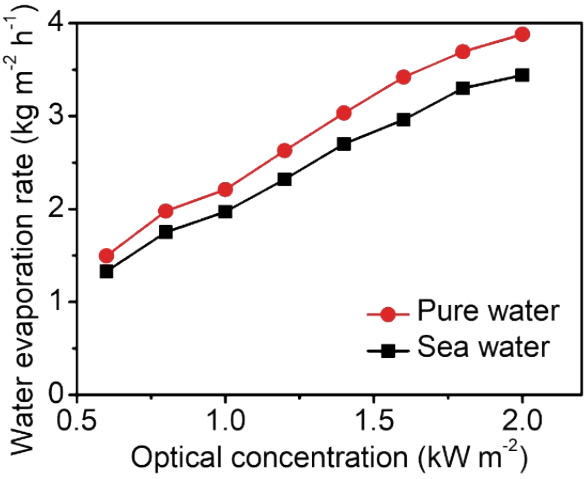

Figure S11. Water evaporation rates of the J-SSG with pure water and sea water, respectively.

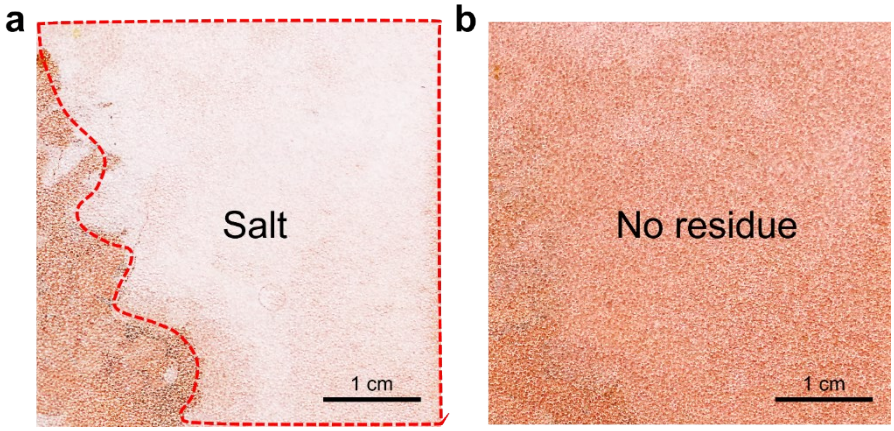

Figure S12. (a) Photograph of the residual salt on the evaporation side of J-SSG after the seawater has completely evaporated. (b) Photograph of the evaporation side of J-SSG after salt removal. The residual salt can be easily washed away.

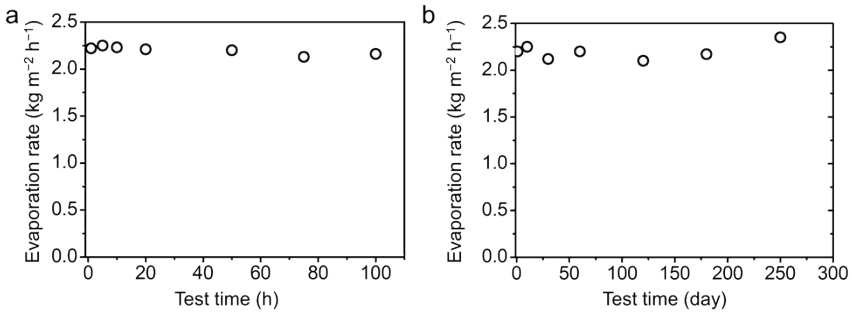

Figure S13. (a) The long-term cycling stability of J-SSG for 100 hours of solar desalination. (b) The reusability of J-SSG. The water evaporation rate of J-SSG remained relatively stable after 250 days.

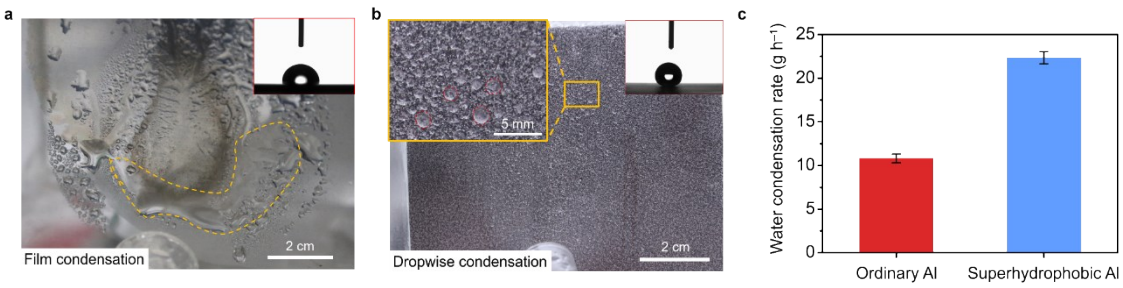

Figure S14. Water condensation performance of metal condenser. (a) Film condensation on the surface of ordinary aluminum condenser. The illustration shows that the water contact angle of ordinary aluminum foil is 95 degrees. (b) Dropwise condensation on superhydrophobic aluminum condenser. The illustration shows that the water contact angle of superhydrophobic aluminum foil is 165 degrees. Related research shows that dropwise condensation has a higher heat transfer power than the film condensation, which makes steam condense faster[3]. (c) Water condensation rate on ordinary aluminum condenser and superhydrophobic aluminum condenser, respectively. We use the same volume of water at 25 ºC to cool the condenser. Then we pass the saturated hot steam to two condensers separately. The condensation rate is obtained by measuring the mass of condensed water over one hour. The superhydrophobic condenser has a higher water condensation rate.

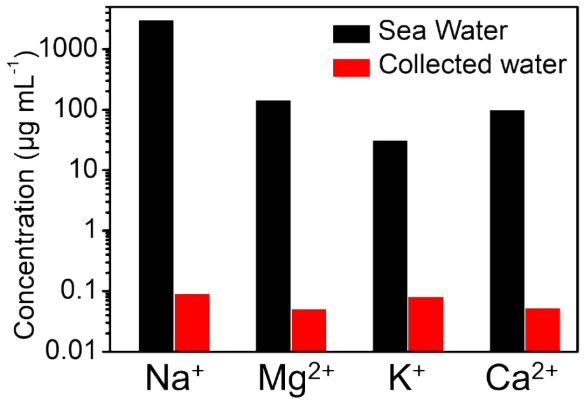

Figure S15. The measured concentrations of four primary positive ions of the sea water and the water desalinated by J-SSG. The Na^+ ions in clean water are *ca.* 0.1 μg mL^{-1}, meaning an ion rejection of 99.9%. The concentrations of K^+, Ca^{2+}, and Mg^{2+} ions are

all below 0.1 μg mL^{-1}, which meets the standard of the World Health Organization for drinking water[4].

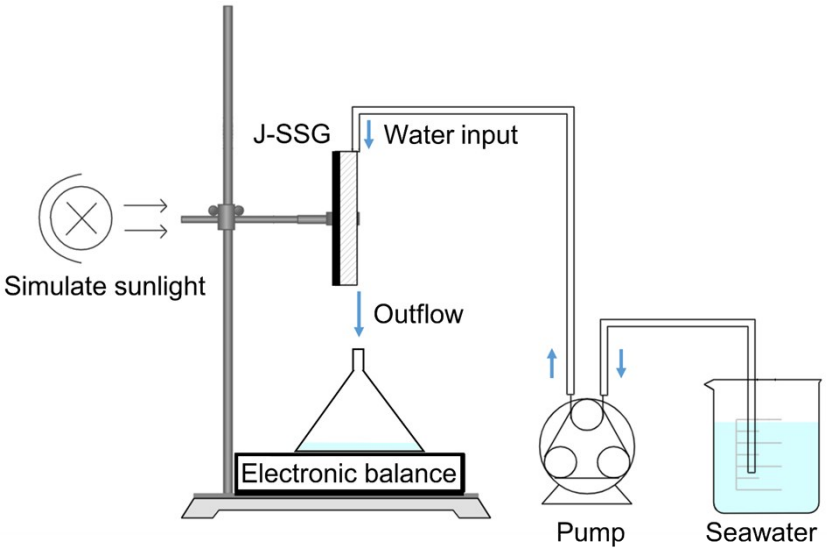

Figure S16. Schematic diagram of J-SSG water evaporation experiment. The amount of input water on J-SSG is measured firstly. The unevaporated water flows out and is weighed by an electronic balance. The water evaporation rate is calculated by the difference between the water supply and the outflow within a certain period of time. The resulting water evaporation rate under light is the result of subtracting dark evaporation.

Theoretical simulation

Note S2 COMSOL Simulation of the temperature field in J-SSG.

Initially, a simulated 3D model with identical size parameters to that of J-SSG was constructed, that is, a cuboid with length and width of 100 mm and height of 3.2 mm. The height of light-absorber side and evaporator side is 0.2 mm and 3.0 mm, respectively. We consider the heat input of 1 sun solar intensity from the solar absorption side, then the heat transfer in the system could be described by the following heat transfer equation[5]:

$$d_z\rho C_P\frac{\partial T}{\partial t} + d_z\rho C_P\vec{u}\cdot\nabla T + \nabla\cdot\vec{q} = d_zQ + q_0 + d_zQ_{ted}$$

$$\vec{q} = -\,d_zk\nabla T$$

Where, ρ is the density, C_p is the heat capacity, T is the temperature, $\vec{u}$ is the flow velocity field, ∇T is the temperature gradient, q is the heat transfer rate, Q is the heat source, Q_{ted} is the increased heat source, $\vec{q}$ is the heat flux vector field, and k is the heat of the substance conductivity, the units are all international units.

The boundary conditions are described by the following equation:

$$q_0 = h(T_{ext} - T)$$

Where, q_0 is the convective heat flux, h is the heat transfer coefficient, T_{ext} is the temperature of the external boundary condition, and T is the temperature of the internal boundary condition, the units are all international units.

The physical properties of each part of the material are in its ideal condition, the porosity of porous copper is 92.5%, and the density is 0.67 kg m^{-3}. Therefore, the temperature distribution in the evaporator in the instantaneous state can be calculated.

Note S3 The energy utilization of solar for water evaporation.

The input sunlight flux is 1000 W m^{-2}, and the energy is converted into three main energy streams: (1) the energy for water evaporation, (2) the reflection energy loss, (3) other ways of heat loss (like heat convection and radiation). The value of the enthalpy of evaporation is obtained through the DSC test (Figure 3i in main text). The enthalpy of evaporation of liquid water in $ACPA_{0.15}$ is about 1532.4 J g^{-1}. Thus, the energy utilization of solar for water evaporation η_s can be calculated by the following equation[6]:

$$\eta_s = \frac{h_v \times WER}{P_{Solar}}$$

Where, h_v is the enthalpy of evaporation of liquid water in $ACPA_{0.15}$, *WER* is the rate of water evaporation, the unit is g m^{-2} s^{-1}, and P_{solar} is the intensity of light. As a result, the energy utilization of solar for water evaporation of J-SSG is approximately 96.5%.

Note S4 COMSOL Simulation of the humidity in J-SSG solar desalination system.

The model is simulated by transforming three-dimensional objects into two-dimensional cross-sections. The modeled structure is shown in Figure 5e in main text, where the J-SSG, moist air, and condenser are presented in narrow bars (red, with widths of 3 mm), right triangle (blue, with length of 10 cm and widths of 4.5cm), and narrow bars (grey, with widths of 1 mm), respectively. In the simulation, we assume the case with water bath condensation as suggested by classical fluid heat transfer.

We assume 1 sun solar intensity energy input to provide energy for water evaporation. Heat is transferred through moist air and transferred to the environment through phase change at the condensation surface. The temperature and humidity fields in this confined space are described by the following equations[7,8]:

The energy change brought about by water evaporation is determined by its enthalpy change:

$$q_{evap} = -L_v g_{evap}$$

$$g_{evap} = K(c_{sat} - c_v)M_v$$

$$c_v = \phi c_{sat}$$

Where, $q_{evap}$is the heat of evaporation, L_v is the enthalpy of evaporation, g_{evap} is the evaporation flux, K is the evaporation rate, c_{sat} is the vapor saturation concentration, c_v is the vapour concentration, ϕ is relative humidity, and M_v is the molar mass of water.

Considering moist air as a turbulence model, the heat transfer equation of moist air is as follows:

$$\rho C_P \vec{u} \cdot \nabla T + \nabla \cdot \vec{q} = Q + Q_p + Q_{vd}$$

$$\vec{q} = - k\nabla T$$

$$M_v \vec{u} \cdot \nabla_{Cv} + \nabla \cdot \vec{g} = G$$

$$\vec{g} = - M_v D \nabla_{Cv}$$

$$q_0 = h(T_{ext} - T)$$

Where, ρ is the density, C_p is the heat capacity, $\vec{u}$ is the flow velocity field, ∇T is the temperature gradient, $\vec{q}$ is the conductive heat flux vector field, Q is the heat source, Q_p is the pressure work, Q_{vd} is the viscous dissipation, k is the thermal conductivity, G contains moisture sources, $\vec{g}$ is the moisture flux by diffusion, D is the vapor diffusion coefficient in air, q_0 is the convective heat flux, h is the heat transfer coefficient, T_{ext} is the temperature of the external boundary condition, and T is the temperature of the internal boundary condition, the units are all international units.

We set up the boundary conditions, the external constant 25 ºC for condensation when using the water cooling.

Table S1 Evaporation performance and actual water productivity performance of our system and previously reported solar desalination systems based on solar-steam generators [9–21].

Solar-steam generator	Solar intensity (kW m^{-2})	Solar absorption (%)	WER (kg m^{-2} h^{-1})	Water evaporation test size (cm^2)	SWP rate (kg m^{-2} h^{-1})	SWP efficiency (%)	Refs.
PPy coated stainless steel mesh	1	98	0.92	~10	0.15	16.3	9
Selective absorber	1	90	--	225	0.55	25	10
Carbon-coated paper	1	~98	1.28	100	0.29	22.6	11
Black cellulose fabric	1	>70	0.84	--	0.33	39	12
3D-Mxene	1	97.5	1.393	1	0.5-0.7	<50	13
PPy	1	94	1.574	~7	0.71	45.1	14
Cu_2SnSe_3	1	96	1.657	~22	0.74	45.2	15
CuxS/Cu	1	~80	1.96	9	0.52(0.6 sun)	45.1	16
Calcinated MS	1	95	1.98	4	0.5-0.8	<40	17
3D-rGO	1	~98	2.10	4	0.8	40	18
rGO	1	~98	2.40	4	1.3	54	19
PVA/rGO hydrogel	1	~98	2.5	1	1.3	52	20
PVA/PPy gel	1	~98	3.2	1	1.6	50	21
J-SSG	1	97	2.21	100	1.95	88	This work

Supplementary References:

[1] K. A. Rocky, M. A. Islam, A. Pal, S. Ghosh, K. Thu, Nasruddin and B. B. Saha, *Appl. Therm. Eng.*, 2020, **164**, 114431.

[2] J. E. Hay and D. C. McKay, *Int. J. Sol. Energy*, 1985, **3**, 203–240.

[3] N. Miljkovic, R. Enright, Y. Nam, K. Lopez, N. Dou, J. Sack and E. N. Wang, *Nano Lett.*, 2013, **13**, 179–187.

[4] F. Edition, *WHO Chron.* 2011, **38**, 104.

[5] M. E. Aalami-Aleagha, B. Hadi and M. A. Shahbazi, *J. Mech. Sci. Techno.*, 2016, **30**, 3767–3776.

[6] P. Zhang, Q. Liao, H. Yao, Y. Huang, H. Cheng and L. Qu, *Energy Stor. Mater.*, 2019, **18**, 429–446.

[7] A. K. Datta, *J. Food Eng.*, 2007, **80**, 80–95.

[8] C. A. Ward and G. Fang, *Phys. Rev. E*, 1999, **59**, 429–440.

[9] L. Zhang, B. Tang, J. Wu, R. Li and P. Wang, *Adv. Mater.*, 2015, **27**, 4889–4894.

[10] T. A. Cooper, S. H. Zandavi, G. W. Ni, Y. Tsurimaki, Y. Huang, S. V. Boriskina and G. Chen, *Nat. Commun.*, 2018, **9**, 5086.

[11] Z. Liu, H. Song, D. Ji, C. Li, A. Cheney, Y. Liu, N. Zhang, X. Zeng, B. Chen, J. Gao, Y. Li, X. Liu, D. Aga, S. Jiang, Z. Yu and Q. Gan, *Glob. Chall.*, 2017, **1**, 1600003.

[12] G. Ni, S. H. Zandavi, S. M. Javid, S. V. Boriskina, T. A. Cooper and G. Chen, *Energy Environ. Sci.*, 2018, **11**, 1510–1519.

[13] X. Fan, Y. Yang, X. Shi, Y. Liu, H. Li, J. Liang and Y. Chen, *Adv. Funct. Mater.*, 2020, **30**, 2007110.

[14] C. Li, D. Jiang, B. Huo, M. Ding, C. Huang, D. Jia, H. Li, C.-Y. Liu and J. Liu, *Nano Energy*, 2019, **60**, 841–849.

[15] Y. Yang, H. Zhao, Z. Yin, J. Zhao, X. Yin, N. Li, D. Yin, Y. Li, B. Lei, Y. Du and W. Que, *Mater. Horizons*, 2018, **5**, 1143–1150.

[16] W. Huang, P. Su, Y. Cao, C. Li, D. Chen, X. Tian, Y. Su, B. Qiao, J. Tu and X. Wang, *Nano Energy*, 2020, **69**, 104465.

[17] F. Gong, H. Li, W. Wang, J. Huang, D. Xia, J. Liao, M. Wu and D. V. Papavassiliou, *Nano Energy*, 2019, **58**, 322–330.

[18] P. Zhang, Q. Liao, H. Yao, H. Cheng, Y. Huang, C. Yang, L. Jiang and L. Qu, *J.*

Mater. Chem. A, 2018, **6**, 15303–15309.

[19] H. Liang, Q. Liao, N. Chen, Y. Liang, G. Lv, P. Zhang, B. Lu and L. Qu, *Angew. Chem. Int. Ed.*, 2019, **58**, 19041–19046.

[20] X. Zhou, F. Zhao, Y. Guo, Y. Zhang and G. Yu, *Energy Environ. Sci.*, 2018, **11**, 1985–1992.

[21] F. Zhao, X. Zhou, Y. Shi, X. Qian, M. Alexander, X. Zhao, S. Mendez, R. Yang, L. Qu and G. Yu, *Nat. Nanotechnol.*, 2018, **13**, 489–495.